Science, Engineering and Social Science Series
ISSN/e-ISSN: 2541 – 0369/2613 – 988X
DOI: -
Vol. 5, No. 1, 2021, Printed in the Indonesia

Numerical FEM Models of Bio-heat Transfer for Magnetic Fluid Hyperthermia Treatments

Febri Dwi Irawati[1,*], Agus Kartono[2]

[1]*Department of Data Science, Institut Teknologi Sumatera*
[2]*Department of Physics, Faculty of Mathematical and Natural Sciences, IPB University*

Numerical solutions using the Finite Element Method (FEM) of healthy one-dimensional bio-heat transfer and cancerous tissue together with the Magnetic Fluid Hyperthermia treatment have been worked out successfully. The bioheat transfer equation was created by modifying the Pennes equation by adding the physiological parameters in each layer. Each layer shows the characteristics of tissue. Each layer represents an independent biological tissue characterized by temperature-dependent physiological parameters and linear temperature-dependent metabolic heat generation. Magnetic fluid hyperthermia (MFH) is used as an external heat source to heat the cancerous area. The magnetic field strength used is 6.5 kA and the frequency of 500kHz in MFH can heat cancer tissue without affecting healthy tissue. In a transient state MFH treatments can heat up cancerous tissue without damaging healthy tissue as indicated by an increase in the temperature of the cancer tissue according to the standard temperature of the MFH treatments.

Keywords: Bio-Heat Transfer, Finite Element Method, Heat Generation, Magnetic Fluid Hyperthermia, Temperature, Tissue.

1. INTRODUCTION

Bioheat transfer is a heat and mass transfer event in the human body that depends on organ systems, blood flow and the thermal response of body tissues to external stimulus [1]. External stimulus that causes thermal responses in cancer therapy are called thermal therapies [2]. The thermal source in thermal therapy is electromagnetic waves [3]. The effect of blood flow on heat transfer in living tissue has been studied for more than a century, one of the experimental studies was conducted by Bernard [4]. Bioheat transfer modeling studies are very useful in the field of thermal-based medicine to predict the temperature distribution in body tissues due to experimental temperature data are not widely available. There are two techniques for measuring body temperature, namely invasive and noninvasive. Invasive temperature measurement techniques tend to be expensive and provide few points of measurement. Non-invasive temperature measurement techniques, such as thermal magnetic resonance imaging, allow volumetric temperature measurement. However, Magnetic resonance imaging has limitations due to high cost and low thermal resolution [5, 6]. Furthermore, Mathematical modeling research on the thermal interactions between blood vessels and tissues has become an interesting research topic. The first quantitative relationship that describes heat transfer in human tissues and the effect of blood flow on tissue temperature is in a continuous manner was presented by Harry H. Pennes, a researcher at the College of Physicians and Surgeons of Columbia University. The equation that he derives is called the Pennes bioheat equation. Pennes was developed by using bioheate equation with heat transfer and blood perfusion, many researchers tried to solve it for a variety of applications, both numerically. and analytically. The solution of the Pennes bioheate equation is obtained with cartesian, cylindrical and spherical coordinates [7, 8, 9]. Durkee et al derived the analytical solution of the classical bioheat equation using eigenfunctions for spherical and cartesian coordinates and cylindrical coordinates [10, 11]. In both cases, a constant heat source is used as a green function to solve the classic bioheat equation for time-dependent sources. Bagaria and Johnson used a variable separation method to obtain a one-dimensional solution to estimate

[*]*Email Address: febri.dwi@sd.itera.ac.id*

the temperature in two concentric spherical regions [12], On the other hand, the source term is described by an exponential function validated experimentally [13]. Rodrigues et al obtained an analytical solution for the one-dimensional Pennes bioheate equation in a multi-layer region that depends on a heat source [14]. Sakrar presents an analytical solution for the steady Pennes bioheate equation in a multi-layer structure [15]. The temperature distribution in each layer is derived separately and the conditions of interface temperature and heat flux compatibility are used to determine the complete solution.

In the last few decades, this Pennes equation has been used to model the magnetic fluid hyperthermia (MFH) cancer therapy [12]. MFH is injecting magnetic nanoparticles immersed in liquid into the target tissue to absorb energy at a higher rate than the surrounding tissue from an externally applied electromagnetic field [16]. Previous research has modeled bioheat transfer under steady state conditions [17]. This study aims to make models and simulations of bioheat transfer in healthy tissue and cancer and to see the temperature distribution of each tissue layer due to the transient thermal response of MFH. The bioheat transfer equation was created by modifying the Pennes equation by adding physiological parameters in each tissue layer. Numerical solutions of equations and simulation of temperature distribution of each network layer using the finite element method.

2. METHODOLOGY

A. Pennes Bio-heat Transfer Equation in Multilayer Tissue

The Pennes equation is used for the analysis of heat transfer in living tissue which describes the effect of blood flow on the temperature distribution in tissues where the absorption or heat source is distributed in a volumetric temperature distribution. This study uses the basic equation. Only the one-dimensional case with constant thermal parameter values is used, which is a good approximation when there is a propagating heat source. The bioheat transfer equation in cartesian coordinates in a multi-layer region is expressed in equation one:

$$\rho_i\, c_i\, \frac{\partial T_i}{\partial t}(x,t) = k_i\, \frac{\partial^2 T_i}{\partial x^2}(x,t) + \omega_{bi}\rho_b c_b\left(T_b - T_i(x,t)\right) + Q_{mi}(x,t) + P_i(x) \quad \textbf{(1)}$$

where $1 \le i \le n,\ x_{i-1} \le x \le x_i$, n is the number of layers. Tissue temperature described by the above equation is controlled by heat storage $\left(\rho_i\, c_i \left(\frac{\partial T_i}{\partial t}\right)\right)$, thermal conduction $\left(k_i \frac{\partial^2 T_i}{\partial x^2}\right)$, heat dissipation through the bloodstream $\left(\omega_{bi}\rho_b c_b\left(T_b - T_i\right)\right)$, and heat generation $\left(P_i\right)$, which represents the contribution of volumetric heat generation, converted from some form of energy such as electromagnetic, ultrasonic or other heating modes. Metabolic heat generation is another type of heat input resulting from the conversion of biochemical energy in the tissue. Here, the rate of metabolic heat generation in the tissue layer and the tissue thermal conductivity are assumed to be uniform while the explanation of the parameter definitions in equation (1) is presented in Table I.

Table I**.** Pennes bioheat transfer equation parameters[1]

Parameter	Unit	Description
ρ	g/cm^3	density of tissue
c	J/g C	heat capacity of tissue
k	W/cm C	the thermal conductivity of tissue
T	^{o}C	temperature of tissue
w_b	s^{-1}	Perfusion of blood
c_b	J/g C	heat capacity of blood
T_b	^{o}C	blood temperature
Q_m	W/cm^3	metabolic heat generation

B. Boundary and Initial Conditions

The first, second and third type boundary conditions with temperatures on the inner and outer surfaces are assumed in equations (2) and (3). The temperature and heat flow must meet the boundary conditions for continuity at the tissue interface stated in equations (6) to (8). The initial temperature depends spatially in the equation (8).

• Inner surface in the first layer $(i=1)$

$$A_{in}\frac{\partial T_1}{\partial x}(x_0,t) + B_{in}\,T_1(x_0,t) = C_{in} \quad \textbf{(2)}$$

• Outer surface of nth layer

$$A_{out}\frac{\partial T_n}{\partial x}(x_n,t) + B_{out}\,T_n(x_n,t) = C_{out} \quad \textbf{(3)}$$

• Inner Interface of ith layer

$$T_i(x_{i-1},t) = T_{i-1}(x_{i-1},t) \quad \textbf{(4)}$$

$$k_i\frac{\partial T_i}{\partial x}(x_{i-1},t) = k_{i-1}\frac{\partial T_{i-1}}{\partial x}(x_{i-1},t) \quad \textbf{(5)}$$

• Outer interface of

$$T_i(x_i,t) = T_{i+1}(x_i,t) \quad \textbf{(6)}$$

$$k_i\frac{\partial T_i}{\partial x}(x_i,t) = k_{i+1}\frac{\partial T_{i+1}}{\partial x}(x_i,t) \quad \textbf{(7)}$$

• Initial conditions

$$T_i(x,t=0) = T_{0i}(x) \quad \textbf{(8)}$$

Parameters in (2) and (3) can be selected to obtain the Dirichlet, Neumann or Robin boundary conditions.

C. Heat generation

The temperature distribution in bioheat transfer is influenced by external stimuli. Cancer patients who undergo treatment will receive an external stimulus, which can be in the form of electromagnetic waves, ultrasonic waves, or magnetic fluid hyperthermia [8]. Bagaria and Johnson describe the external stimulus as a polynomial equation

$$P = P_0 + P_1 x + P_2 x^2 \quad \textbf{(9)}$$

where P_0, P_1, and P_2 are constants [6]. Heat source parameter values for the four cases are shown in Table II.

Table II. Value of heat generation parameters for six cases

Case	P_0 $\left(W/cm^3\right)$	P_1 $\left(W/cm^4\right)$	P_2 $\left(W/cm^5\right)$	P_{const} $\left(W/cm^3\right)$
1	0.7	-1.4	0.7	0.07
2	0.3	-0.2	-0.1	0.09
3	0.1	0.5	-0.6	0.115
4	0.5	-0.2	-0.3	0.17
5	0.0	1.5	-1.5	0.225
6	0.1	0.8	-0.7	0.28

Salloum experimentally described the external stimulus in the form of a Gaussian distribution [13].

$$P = Ae^{-x^2/x\phi^2} \quad \textbf{(10)}$$

where x is the radial distance from the injection site, x_ϕ is a parameter that determines how far the nanoparticles are spread from the injection site, and A is the maximum force of the volumetric heat generation rate (W/cm^3).

D. Numerical Solution Title, Authors Name & Affiliation

The approximate solution of the 2-1 bioheat transfer equation first discretizes the line domain Ω into a number of finite elements, the element nodes are located at the positions x_j, for $j=1,\ldots,N+1$, where $x_1=0$ and $x_{N+1}=L$, as shown in Figure 1. In each element a certain point is identified which is called the vertex or nodal which will play an important role in the formation of the finite element [19]. A collection of elements and vertices forming a domain is called a finite element mesh (see Figure 1).

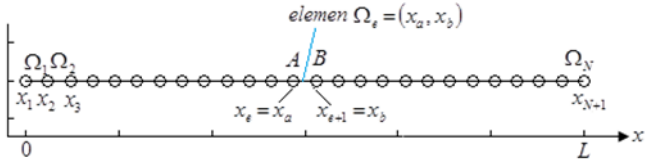

Figure 1. Discretization of the finite element or one dimensional domain for model problems

The *j*th Galerkin projection of equation is expressed in equation 11.

$$\rho_i c_i \int_{x_a}^{x_b} \phi_j \frac{\partial T_i}{\partial t}\,dx = -k_i\left(\phi_j \frac{\partial T_i}{\partial x}\right)_{x=x_a} + k_i\left(\phi_j \frac{\partial T_i}{\partial x}\right)_{x=x_b} - k_i \int_{x_a}^{x_b} \frac{\partial \phi_j}{\partial x}\frac{\partial T_i}{\partial t}\,dx + \omega_{bi}\rho_b c_b \int_{x_a}^{x_b} \phi_j T_b\,dx - \omega_{bi}\rho_b c_b \int_{x_a}^{x_b} \phi_j T_i\,dx + \int_{x_a}^{x_b} \phi_j Q_{mi}\,dx + \int_{x_a}^{x_b} \phi_j P_i(x)\,dx \quad \textbf{(11)}$$

where the index *j* runs over an appropriate number of nodes determined by the degree of the element interpolation functions and by the specified boundary conditions Dirichlet and Neumann. Substitute equation the finite element expansion of the numerical solution,

$$T(x) = \sum_{l=1}^{N_E} T_l(t)\phi_l(x) \quad \textbf{(12)}$$

and a corresponding expansion for heat generation

$$P(x) = \sum_{l=1}^{N_E} P_l(t)\phi_l(x) \quad (13)$$

where N_E is a number of unique global node. Rearranging and collecting all nodal projections, derive a system of linear ordinary differential equations (ODEs),

$$\mathbf{M}\cdot\frac{d\mathbf{T}}{dt} + \kappa\,\mathbf{D}\cdot\mathbf{T} = \kappa\,\mathbf{b} \quad \textbf{(14)}$$

where $\mathbf{T}$ is the vector of the unknown temperature at each node.

$$T \equiv \left[T_1,\ T_2,\ \ldots,\ T_{N_E-1},\ T_{N_E}\right]^T \quad \textbf{(15)}$$

where M is a global square mass matrix, $\mathbf{D}$ is a global square diffusion matrix, and $\mathbf{b}$ is a properly constructed right-hand side.

$$M \equiv \begin{bmatrix} \frac{1}{3}h_1 & \frac{1}{6}h_1 & 0 & 0 & \ldots \\ \frac{1}{6}h_1 & \frac{1}{3}h_1+\frac{1}{3}h_2 & \frac{1}{6}h_2 & 0 & \ldots \\ 0 & \frac{1}{6}h_2 & \frac{1}{3}h_2+\frac{1}{3}h_3 & 0 & \ldots \\ \vdots & 0 & \cdots & \cdots & \cdots \\ \vdots & \vdots & \vdots & \vdots & \vdots \\ 0 & \cdots & \cdots & \cdots & \cdots \end{bmatrix} \begin{bmatrix} 0 & 0 & 0 \\ 0 & \cdots & 0 \\ \cdots & 0 & 0 \\ \frac{1}{3}h_{N_E-3}+\frac{1}{3}h_{N_E-2} & \frac{1}{6}h_{N_E-2} & 0 \\ \frac{1}{6}h_{N_E-2} & \frac{1}{3}h_{N_E-2}+\frac{1}{3}h_{N_E-1} & \frac{1}{6}h_{N_E-1} \\ 0 & \frac{1}{6}h_{N_E-1} & \frac{1}{3}h_{N_E-1}+\frac{1}{3}h_{N_E} \end{bmatrix} \quad (16)$$

Galerkin finite element system form

$$\frac{1}{3}h_1\frac{dT_1}{dt} + \frac{1}{6}h_1\frac{dT_2}{dt} + \kappa\sum_{l=1}^{N_E} D_{1,l}T_l = \kappa b_1 \quad \textbf{(17)}$$

and

$$\frac{1}{6}h_{j-1}\frac{dT_{j-1}}{dt} + \frac{1}{3}\left(h_{j-1}+h_j\right)\frac{dT_j}{dt} + \frac{1}{6}h_j\frac{dT_{j+1}}{dt} + \kappa\sum_{l=1}^{N_E} D_{1,l}T_l = \kappa b_j \quad \textbf{(18)}$$

for $j = 2, \ldots, N_E$, Rearranging (18)

$$\left(\frac{1}{3}\frac{h_{j-1}}{h_{j-1}+h_j}\right)\frac{dT_{j-1}}{dt}+\left(\frac{2}{3}\right)\frac{dT_j}{dt}+\left(\frac{1}{3}\frac{h_j}{h_{j-1}+h_j}\right)\frac{dT_{j+1}}{dt}+\kappa\frac{2}{h_{j-1}+h_j}\sum_{l=1}^{N_E}D_{j,l}T_l=\kappa\frac{2}{h_{j-1}+h_j}b_j \quad \textbf{(19)}$$

For $j = 2, \ldots, N_E$.The first three terms on the left-hand side of (19) contribute a weighted average of the time derivative at three neighboring nodes. The sum of the weights enclosed by the parentheses is equal to unity. When the element size is uniform, $h_1 = h_2 = \cdots = h_{N_E} \equiv h$, the Galerkin equations simplify to

$$\frac{1}{3}\frac{dT_1}{dt}+\frac{1}{6}\frac{dT_2}{dt}=\kappa\frac{T_2-T_1}{h^2}+\frac{\kappa}{h}b_1 \quad (20)$$

and

$$\frac{1}{6}\frac{dT_{j-1}}{dt}+\frac{2}{3}\frac{dT_j}{dt}+\frac{1}{6}\frac{dT_{j+1}}{dt}=\kappa\frac{T_{j-1}-2T_j+T_{j+1}}{h^2}+\frac{\kappa}{h}b_j \quad (21)$$

for $j = 2, \ldots, N_E$. The first term on the right-hand side of (21) is recognized as the central difference approximation of the second derivative, $\partial^2 T / \partial x^2$, evaluated at the *j*th node. The three terms on the left-hand side express a weighted average of the time derivative at the ith and adjacent nodes. A similar averaging of the source function is implicit in the constant term on the right-hand side, b_j. Equation (2 to 14) provides us with a coupled system of first-order, linear, ordinary differential equations (ODEs) in time, t, for the unknown node temperatures, $T_i(t)$. The coupling of nodal temperatures on the left-hand side mediated through the global mass matrix. The system (2-14) is integrated in time using a numerical Crank–Nicolson method for solving initial-value problems involving ordinary differential equations [18,19].

$$\mathbf{M}\cdot\frac{\mathbf{T}^{(n+1)}-\mathbf{T}^{(n)}}{\Delta t}+\frac{1}{2}\kappa\,\mathbf{D}\cdot\left(\mathbf{T}^{(n)}+\mathbf{T}^{(n+1)}\right)=\frac{1}{2}\kappa\left(\mathbf{b}^{(n)}+\mathbf{b}^{(n+1)}\right) \quad \textbf{(22)}$$

Rearranging, derive a linear algebraic system,

$$\mathbf{C}\cdot\mathbf{T}^{(n+1)}=\boldsymbol{r} \quad \textbf{(23)}$$

The tridiagonal coefficient matrix on the left-hand side is given by

$$\mathbf{C}=\mathbf{B}+\frac{1}{2}\kappa\,\Delta t\,\boldsymbol{D} \quad \textbf{(24)}$$

and the right-hand side is given by

$$\boldsymbol{r}=\left(\mathbf{M}-\frac{1}{2}\kappa\,\Delta t\,\boldsymbol{D}\right)\cdot\mathbf{T}^{(n)}+\frac{1}{2}\kappa\,\Delta t\left(\mathbf{b}^{(n)}+\mathbf{b}^{(n+1)}\right) \quad \textbf{(25)}$$

3. RESULT AND DISCUSSION

Comparison between the transient temperature profile for a uniform heat source which is called constant heat generation and a non-uniform heat source which is called quadratic heat generation. The heat source is assumed to be in the tumor tissue with a tissue length of 1 cm. In this condition the network is considered one layer. The material property used in this calculation is magnetite, monodisperse with a diameter of 12 nm. The magnetic field strength used is 6.5 kAm^{-1} and a frequency is 500kHz. Bioheat parameter values used are $\rho_b = 1000\,{}^{kg}/_{m^3}$, $c_b = 4200\,{}^{J}/_{kg\,^oC}$, $T_b = T_c = 37\,^oC$, $\omega_b = 0.0005\,ml/s/ml$, $Q_{m_1} = 0\,{}^{W}/_{m^3}$, and $k_1 = 0.55\,{}^{W}/_{m\,^oC}$. The temperature boundary conditions parameters on the inner and outer surface are $A_{in} = 0\,{}^{W}/_{cm\,C}$, $B_{in} = 1\,{}^{W}/_{cm^2\,C}$, $C_{in} = \hat{C}\,{}^{W}/_{m^2}\left(\hat{C} \in \Re\right)$, $A_{out} = 0$, $B_{out} = 1$, $C_{out} = 37\,^{o}\mathrm{C}$. The number of elements used in the numerical solution is 25 elements. The value Δt used for $t = 100\,s$ and $t = 100\,s$ for each $0.2\,s$ iteration. In this figure, the temperature distribution of the steady state is higher than the transient, because in a steady state the temperature does not change with time or in other words it is constant. In transient conditions or also called temporary conditions, the temperature will change over time. The temperature when it is above the ideal minimum temperature is hyperthermia, this can indicate that the time needed to heat the tumor tissue measuring 1 cm is 300 s.

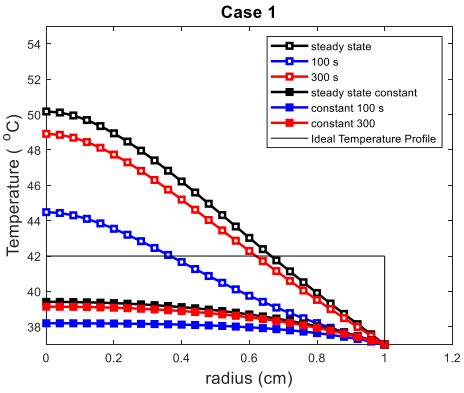

(a)

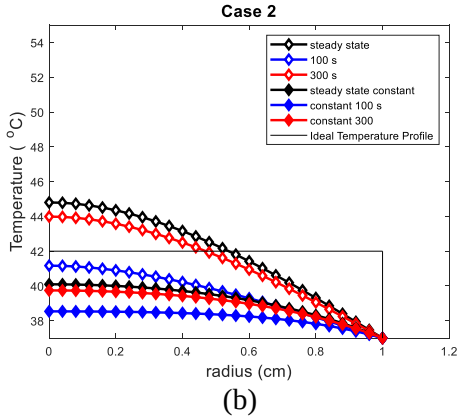

(b)

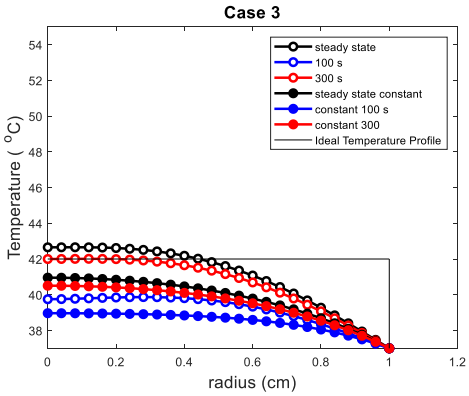

(c)

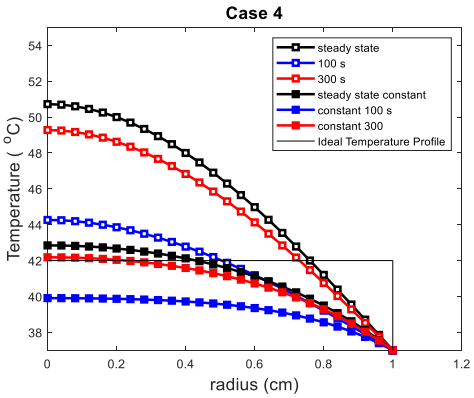

(d)

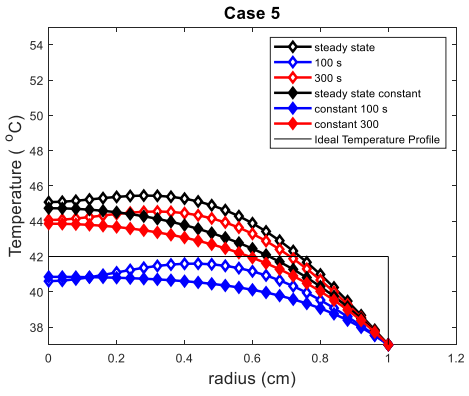

(e)

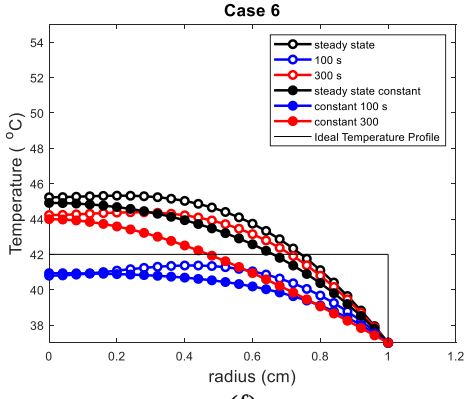

(f)

Figure 2. Single layer temperature distribution profile with constant and quadratic heat source for transient state

Here, Figure 3 shows the comparison of transient temperature profiles for constant heat generation and quadratic heat generation on two layers, namely tumor tissue and healthy tissue. The parameter values used are $\rho_1 = 1.1\, g\, cm^{-3}$, $\rho_2 = 1\, g\, cm^{-3}$, $\rho_b = 1\, g\, cm^{-3}$, $c_1 = c_2 = c_b = 4.2\, J\, kg^{-1}\, {}^{o}C^{-1}$, $T_b = T_c = 37\, {}^{o}C$, $\omega_{b_1} = \omega_{b_2} = 5\times10^{-3} s^{-1}$, $Q_{m_1} = Q_{m_2} = 0\, W\, cm^{-3}$, $k_1 = 5.5\times10^{-3}\, W\, cm^{-1}\, {}^{o}C^{-1}$, $k_2 = 5\times10^{-3}\, W\, cm^{-1}\, {}^{o}C^{-1}$. The temperature boundary conditions parameters on the inner and outer surface are as follows $A_{in} = 0$, $B_{in} = 1$, $C_{in} = \hat{C}\ \left(\hat{C} \in \Re\right)$, $A_{out} = 0$, $B_{out} = 1$, $C_{out} = 37\ {}^{o}\mathrm{C}$. The number of elements used in the numerical solution is 100 elements. The value Δt used for $t = 100\, s$ and $t = 300\, s$ is $0.2\, s$ for each iteration. The two-layer condition also shows the temperature distribution, a steady state, is higher than the transient. The temperature at the two layers in the tumor tissue is not different from Figure 2. In the figure, it can be seen that the healthy tissue which is located close to the tumor tissue has an increase in temperature but is below the ideal temperature of hyperthermia so that it does not damage and affect the nature of the healthy tissue. When $t = 300\, s$ is seen that the temperature rises with an increase in temperature to the ideal minimum of hyperthermia, this can indicate that the time needed to heat 4 cm of tissue is 300 s.

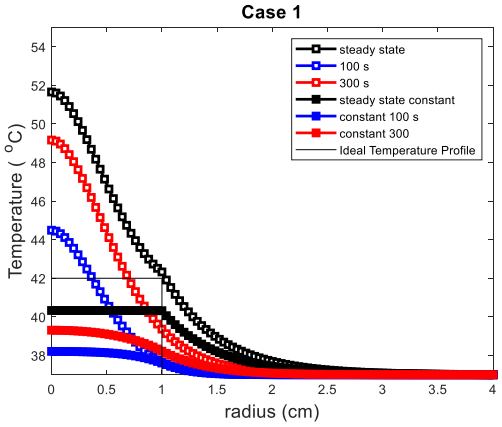

(a)

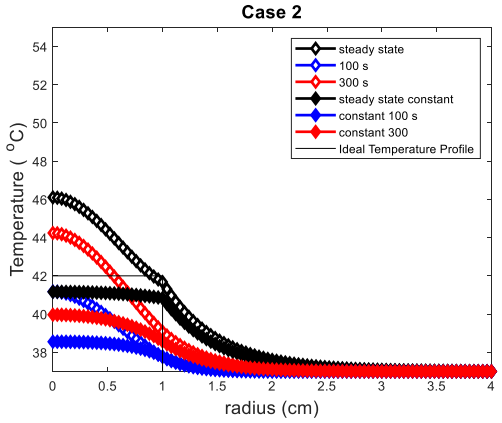

(b)

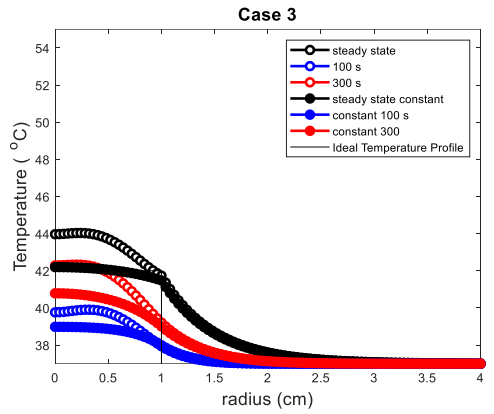

(c)

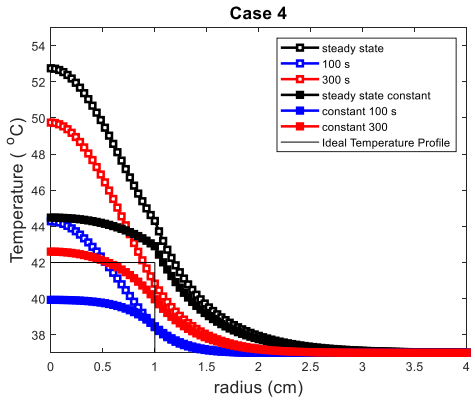

(d)

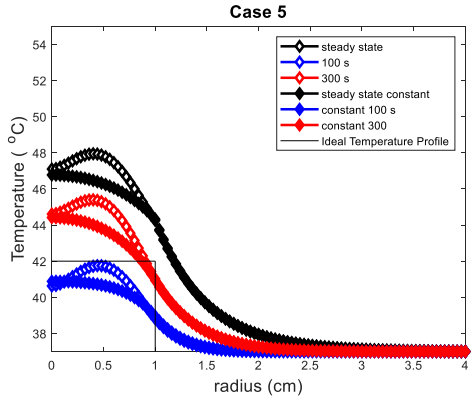

(e)

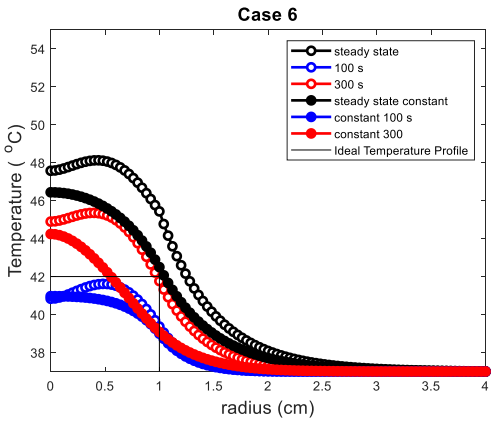

(f)

Figure 3. Two-layers temperature distribution profile with constant and quadratic heat source for transient state

Model validation is done by comparing the results of the model that describe bioheat transfer with the analytical results. The analytical results were obtained from the results of the reduction by Zhong-Shan Deng. The result of reduction by ZhongShan Deng is a bioheat transfer equation for one layer so that the boundary conditions of the inner and outer layers of the layer are not used for this model. The model results were also validated with the results of the MFH experiment from Salloum et al. The experiment was conducted to measure the temperature in the hind limb muscle tissue of mice induced by injection of magnetic nanoparticles during the in vivo MFH experiment [12].

4. CONCLUSIONS

This study managed to develop a model that uses a transfer bioheat Pennes basic equation that describes the transfer of heat to healthy tissue and cancer cells as well as therapies are MFH. This shows that the model created can be used to calculate the temperature distribution under various other boundary conditions and that several tissue layers have been used in this model. Transient temperature distribution simulations on a tissue with one layer and two-layer variations using the finite element method have also been successfully carried out. MFH treatment on tissue causes an increase in temperature in cancer tissue and does not affect healthy tissue.

References

[1] Pennes H. **(1948)**. Analysis of tissue and arterial blood temperatures in the resting human forearm. J. Appl. Physiol. 1 (2) : 93–122. doi : 9714612

[2] Sheu Tony W.H, Maxim A. Solovchuk, Alex W.J. Chen, Marc Thiriet. **(2011)**. On an acoustics–thermal–fluid coupling model for the prediction of temperature elevation in liver tumor. Int J Heat Mass Transfer. 54: 4117–4126. doi: 10.1016/ j.ijheatmasstransfer.2011.03.045.

[3] Habash RWY, Bansal R, Krewaski D, Alhafid HT. **(2006)**. Thermal therapy part-I: an introduction to thermal therapy. Crit Rev Biomed Eng. 34(6):459–489.

[4] Bernard M Claude. **(1876)**. Lecons sur la chaleur animale sur les effets de la chaleur et sur la fievre. Paris : Avec Figures Intercalees Dans Le Text.

[5] Craciunescua O.I, P.R. Stauffer, B.J. Soher, C.R. Wyatt, O. Arabe, P. Maccarini, S.K. Das, K.S. Cheng, T.Z. Wong, E.L. Jones, M.W. Dewhirst, Z. Vujaskovic, J.R.MacFall. **(2009)**. Accuracy of real time noninvasive temperature measurements using magnetic resonance thermal imaging in patients treated for high grade extremity soft tissue sarcomas. Med. Phys. 36 : 4848 – 4858. doi : 10.1118/1.3227506.

[6] Gallermann J, W. Wlodarczyk, A. Feussner, H. Fahling, J. Nadobny, B. Hildebrandt, R. Felix, P. Wust. **(2005)**. Methods and potentials of magnetic resonance imaging for monitoring radiofrequency hyperthermia in a hybrid system. Int. J. Hyperther. 21(6) : 497–513. doi : 10.1080/02656730500070102.

[7] Giordano M A, G. Gutierrez, C. Rinaldi. **(2010)**. Fundamental solutions to the bioheat equation and their application to magnetic fluid hyperthermia. Int. J.Hyperther. 26 (5): 475–484. doi : 10.3109/02656731003749643.

[8] Lin CT, K.C. Liu. **(2009)**. Estimation for the heating effect of magnetic nanoparticles in perfused tissues. Int. Commun. Heat Mass Transfer. 36: 241–244. doi : 10.1016/j.icheatmasstransfer.(2008).11.006.

[9] Okajima Junnosuke, S. Maruyama, H. Takeda, A. Komiya. **(2009)**. Dimensionless solutions and general characteristics of bioheat transfer during thermal therapy, J. Therm.Biol. 34: 377–384. doi : 10.1016/j.jtherbio.2009.08.001.

[10] Durkee J.W, P.P. Antich, C.E. Lee. **(1990)**. Exact-solutions to the multiregion timedependent bioheat equation 1: solution development. Phys. Med. Biol. 35(7): 847–867. doi: 0031-9155/35/7/004.

[11] Durkee J.W, P.P. Antich. **(1991)**. Characterization of bioheat transport using an exact solution to the cylindrical geometry, multiregion, time-dependent bioheat equation. Phys. Med. Biol. 36(10): 1377–1406. doi: 0031-9155/36/10/006Bagaria, 2005

[12] Salloum M, R.H. Ma, L. Zhu. **(2008)**. An in-vivo experimental study of temperature elevations in animal tissue during magnetic nanoparticle hyperthermia. Int J Hyperther. 24(7): 589–601. doi : 10.1080/02656730802203377.

[13] Rodrigues D B, P.J.S. Pereira, P. Limão-Vieira, P.R. Stauffer, P.F. Maccarini. **(2013)**. Study of the one dimensional and transient bioheat transfer equation: Multi-layer solution development and applications. Int J Heat Mass Transfer. 62:153–162.

[14] Sarkar Daipayan, A. Haji-Sheikh, Ankur Jain. **(2015)**. Temperature distribution in multi-layer skin tissue in presence of a tumor. Int J Heat Mass Transfer. 91 : 602–610. doi : 10.1016/j.ijheatmasstransfer.2015.07.089.

[15] Gilchrist RK, Medal R, Shorey WD, Hanselman RC, Parrott JC, Taylor CB. **(1957)**. Selective inductive heating of lymph. Ann Surg. 146:596–606.

[16] Kartono A. Febri Dwi I, Tony S. **(2018)**. Numerical solution of one-dimensional bio-heat transfer on human head tissue problem by finite element method. JP Journal of Heat and Mass Transfer. 15: 433 – 456. doi : 10.17654/HM015020433.

[17] Sheu Tony W.H, Maxim A. Solovchuk, Alex W.J. Chen, Marc Thiriet. **(2011)**. On an acoustics–thermal–fluid coupling model for the prediction of temperature elevation in liver tumor. Int J Heat Mass Transfer. 54: 4117–4126. doi: 10.1016/ j.ijheatmasstransfer.2011.03.045.

[18] Pozrikidis, Constantine. **(2014)**. Introduction to Finite and Spectral Element Methods Using MATLAB. Second Edition-CRC Press.,

Received: 9 December 2020, Accepted: 8 February 2021